Jurnal Teknologi

Full Paper

RESPONSE OF FBG–BONDED PLASTIC PLATE AT DIFFERENT LOCATIONS OF APPLIED STRESS

Younis Mohammed Salih*, Yusof Munajat, Abd Khamim Ismail, Hazri Bakhtiar

Department of Physics, Faculty of Science, Universiti Teknologi Malaysia, 81310 UTM Johor Bahru, Johor, Malaysia

Article history
Received
1 February 2015
Received in revised form
24 March 2015
Accepted
1 August 2015

*Corresponding author
younis20000@gmail.com

Graphical abstract

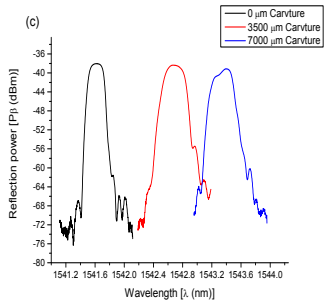

Abstract

Fiber Bragg Grating sensing (FBG) has been intensively studied in the application of smart structures because of its immense advantages offered over those of the conventional sensors. In these researches unique characteristics of FBG, like its high sensitive resonance frequency spectrum and its resonant behavior were reported when FBG was coated by a ring-shaped material and used as an underwater acoustic sensor. In this study, the response of a FBG-bonded plastic plate at different locations of applied stress is demonstrated. The sensing element utilized for this purpose is a 10 *mm* FBG sensor bonded onto the surface of a plastic plate. Results of reflection spectrum showed that the output power increased randomly when the location of applied stress approached the location of FBG. This was assured from the increment of the area of reflection spectrum. The random increase in the output voltage was attributed to the insufficient stiffness of the plastic ruler, suggesting the implement of graphene plate instead of plastic ruler and increasing the grating length of FBG. The results showed an increase in the output power as detected by the photodiode. Consequently, a clear correlation between the optical and electrical outputs was observed.

Keywords: Acoustic sensor; fiber Bragg grating; shift in Bragg wavelength

1.0 INTRODUCTION

The Fiber Bragg Grating (FBG) is fabricated by constructing periodic or quasi periodic changes in the refractive index of the core along a single mode optical fiber length, as illustrated in Figure 1.

This periodic change in refractive index is typically created by exposing the core to an intense optical interference pattern of ultraviolet energy, after which the pattern is printed into the fiber as shown in Figure 2. The formation of permanent grating structures in optical fiber was first demonstrated by Hill et al., (1978) at the Canadian Communications Research Centre (CRC) in Ottawa, Ontario, Canada [1–4].

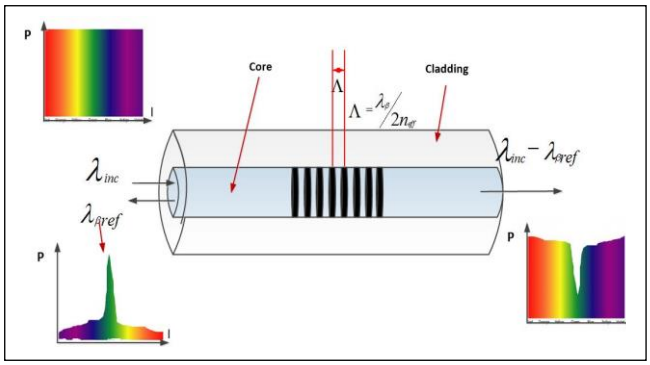

Figure 1 Illustration of a uniform Bragg grating with constant index of modulation amplitude and period

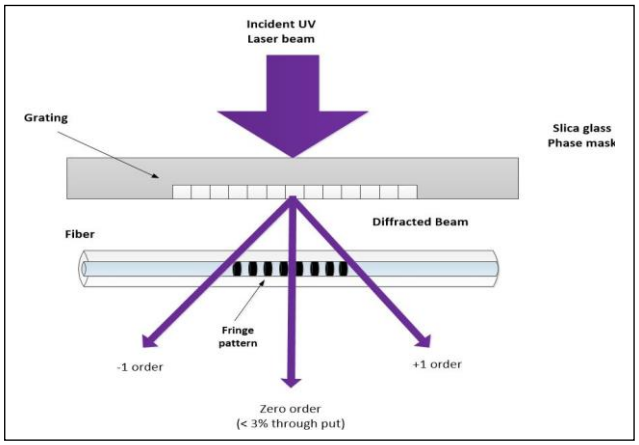

Figure 2 The formation of permanent grating structures in optical fiber

These make uniform fiber gratings, where the phase fronts are perpendicular to the fibers longitudinal axis with grating planes. The Bragg grating condition is simply the requirement that satisfies both energy and momentum conservation. The first-order Bragg condition is defined as [5]:

$$\lambda_\beta = 2\, n_{eff}\ \Lambda \qquad (1)$$

Where

λ_β = Bragg wavelength; Λ = Grating period; n_{eff} = Effective refractive index of the grating in the fiber core.

Based on its unique characteristics, FBGs have proven to be ideal for a variety of applications. Examples include, diverse construction processes [6–8], maintenance in flight monitoring and space vehicles, marine and medical science [9, 10]. According to literature, its wide application area has been mainly attributed to its ability to keep its reflectivity under radiation exposure [12], its immunity to electromagnetic interference, and applications in remote sensing, stability in harsh environments, multiplexing capability, high sensitivity, wide dynamic range and simplicity.

In the past decade, many researchers have tried to enhance the sensitivity of FBGs by using many methods. For example, [13] used optical isolators before and after the FBG fiber, while [14] used a SPC connector fiber for the termination of the FBG sensor in the reflection mode with an optical circulator between the FBG and optical source to rectify the instability in the output signal. Also, based on the design of [11], they reported that the cantilever sensor exhibited a high sensitive resonance frequency spectrum. Subsequently, [12] used a Cu-coated fiber to develop a FBG acoustic sensor for integrated structural health monitoring (ISHM) of nuclear power plant (NPP). By carrying out a full 3-D numerical analysis and experimental verification of an acoustic sensor in the frequency range 0.5-30 kHz, [15] reported the first evidence of the resonant behavior of an underwater acoustic sensor constituted by an FBG coated by a ring-shaped material. Hence, in this research work, the response of a FBG-bonded plastic plate at different locations of applied stress is investigated. The sensing element utilized for this purpose is a 10 *mm* FBG sensor bonded onto the surface of a plastic plate.

1.1 Effect of Acoustic and Ultrasonic on FBG

From Eq. (1) a change in the Bragg wavelength λ_β can be achieved by either a change in the grating period, Λ, or a change in the effective refractive index, n_{eff} That is,

$$\Delta\lambda_\beta = 2n\Delta\Lambda + 2\Lambda\Delta\, n_{eff} \qquad (2)$$

For the specific case of pure axial loading, the shift in Bragg wavelength is linearly related to the applied axial strain that can be written as,

$$\Delta\lambda_\beta = \lambda_\beta\ (1 - P_e)\epsilon \qquad (3)$$

Where P_e is the effective photo-elastic constant for axial strain with a typical value 0.22

From Eq. (3) FBGs are typically utilized as spectral transduction elements, where the change in the measurement is detected via a shift in the peak wavelength of the FBG (in the case of hydrophones) or in the form of a strain wave (for mechanical vibrations). These are converted into the shift in the wavelength, which can be easily determined via an interrogator [16, 18].

1.2 Interrogation Methods

For the acoustic wave detection, we need new fast interrogation system. The working principle of fiber optic sensor using FBG (Fiber Bragg Grating) is shown in Figure 3. Also, for more illustration, a transmission spectrum is shown in Figure 4. One can notice from the figures that when the Bragg wavelength is increased, the transmitted intensity is decreased.

Meanwhile, the reflected or rejected intensity, Ir is going to be increased correspondingly.

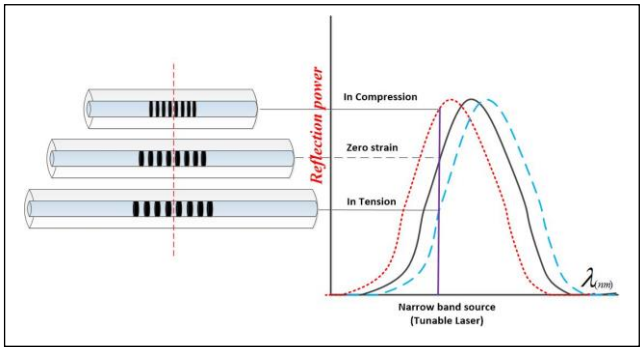

Figure 3 Measuring principle of FBG sensor

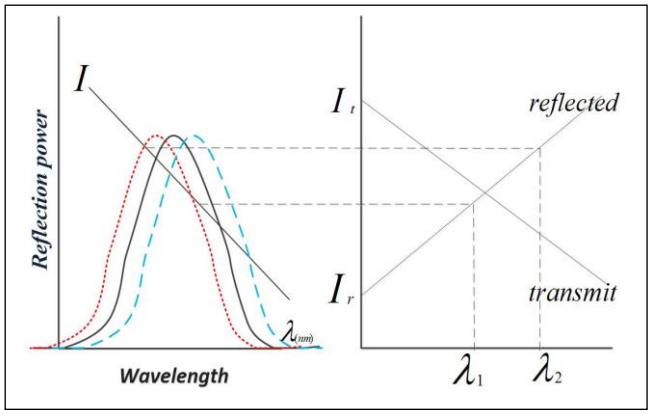

Figure 4 Demodulating FBG with a passive filter. Wavelength shifts (left) are converted into intensity changes (right) [17]

Lee and Jeong, (2002), were mentioned many interrogation techniques for fiber grating sensors and the theory of fiber gratings [12]. Essentially, two broad interrogation methods are available for the detection of high frequency acoustic signal with FBGs which are, power detection methods, and edge filter detection methods [16].

1.2.1 Power Detection Methods

In the power detection method, as used in this work, the shift in the FBG peak wavelength (the Bragg wavelength) is detected due to the spectral properties of the Light Source (LS). By utilizing the power detection methods, the FBG acts as a filter that splits the incident optical power into the reflected and transmitted components. Upon the application of stress and changes occurred in the Bragg wavelength, the total transmitted and reflected powers are subjected to change [18]. The power changes can be readily detected by means of two sources, which are the linear edge source [25] and the narrow bandwidth source [19].

In the linear edge source, to realize the power detection (see Figure 5(a)), the edge of a relatively broadband source (source bandwidth > FBG bandwidth) and the FBG are chosen such that the Bragg wavelength is located at the 3 dB point of the source. The wavelength shift of the FBG will then produce a direct change in the reflected intensity as it shifts up and down the edge of the source's spectrum [16].

The second power detection method is opposite to that of the linear edge source (see Figure 5(b)). In this case, a relatively narrow bandwidth source (source bandwidth < FBG bandwidth) is set to the 3 dB point of the FBG. Here, either the reflected power [19] or the transmitted power can be utilized [13].

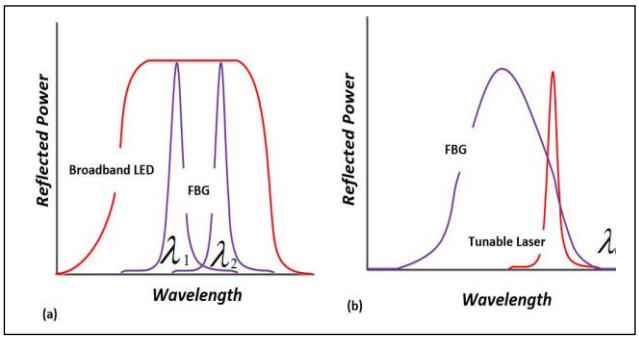

Figure 5 FBG detection method using: (a) a broadband light emitting diode; (b) a narrow line-width tunable laser source [18]

1.2.2 Edge Filter Detection Methods

In edge detection method, a spectrally-dependent filter, which results in the change in intensity at the detector, is used to detect the shift in the FBG spectrum. Illumination of the FBG is done by a broadband source like SLD. The change in the reflected wavelength causes the transmitted intensity to vary when the filters transmittance is varied as a function of wavelength. The types of filters that can be utilized include a matched FBG [21], a wavelength division multiplexing (WDM) coupler [22], an arrayed-waveguide (AWG) [23] and a dense division multiplexing (DWDM) filter [24].

The most straight-forward of the edge filter detection methods is the linear edge absorption filter because an external filter is used. While, the simplest form of the edge filter is a matched FBG. In this case, an identical FBG is used as the filter, which converts the spectral shift of the FBG into an intensity change. Other two edge filter detection methods are AWG and DWDM filters that are both multichannel devices and are thus, identical in their implementation [16].

2.0 METHODOLOGY

2.1 Preparation of FBG-bonded Sensor

To prepare FBG-bonded sensor, the surface of a (800 x 1 x 260) *mm*^{2} *(l x w x h)* plastic plate was bonded by a10-*mm* FBG sensor. This has been done by using a specified adhesive material in the type of SELLEEYS to bond the FBG horizontally on the plastic ruler, as shown in Figure 6.

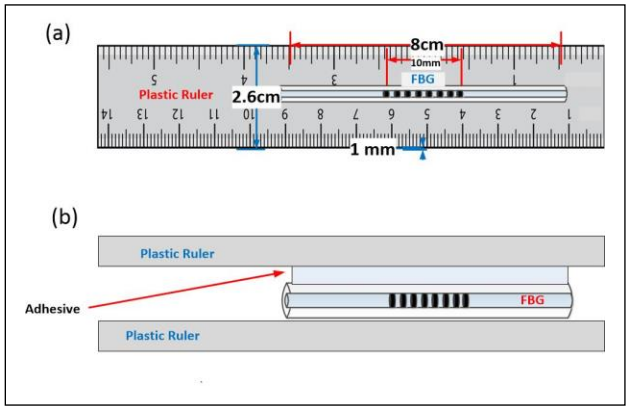

Figure 6 FBG bonded on plastic plate. (a) Ruler, and FBG dimensions. (b) Explanation FBG bonded on plastic rulers

2.1 Tension and Curvature Effect on FBG

An external power source (ALS-18-B-FA ASE) with a spectral range from 1528 *nm* to 1564 *nm*, operating at maximum power, was used as a light source (LS) for the investigation of the effect of tension and curvature on FBG (1541.8 *nm*). Port 1 and port 2 of a circulator were connected to the LS and the FBG sensor, respectively. As such, by means of changing the displacement in linear translation stage (in steps of 500 μm), the reflection spectrum of the disturbed FBG has been obtained in two ways; i) by using an optical spectrum analyzer (OSA) and ii) by using a high-speed photo diode connected with an oscilloscope.

In the first stage of the experiment, the lateral displacement was changed from 0 to 7000 μm in steps of 500 μm in accordance to the increase or decrease in the FBG's curvature. For the stress location at 1 cm away from the end of the FBG region, the change in wavelength center, λ_β (Bragg wavelength shift caused by tension and curvature) of the FBGs was recorded in *nm*. Moreover, the experimental procedure was repeated for stress locations at 2 cm and 3 cm. The reflected spectrum was recorded for two different lateral displacements (0, 3500 μm and 7000 μm). Throughout the experimental investigations, an optical spectrum analyzer (OSA) (Yokogawa AQ6370C) was utilized. The experimental setup for the determination of the response of tension and curvature on the FBG is shown in Figure 7.

In the second part of the experiment, a high-speed photo diode coupled with an oscilloscope was used instead of OSA. Variation in the mean voltage was recorded at similar lateral displacements mentioned before, as well as at the corresponding increase and decrease in the curvature of the FBG. The discrete lines shown in Figure 7 define the way of obtaining the curvature tension of the FBG. The High-Speed photo diode used was DET01CFC, operating in the wavelength range from 800 to 1700 *nm*, while the oscilloscope used was in the type of REGOL DS2000.

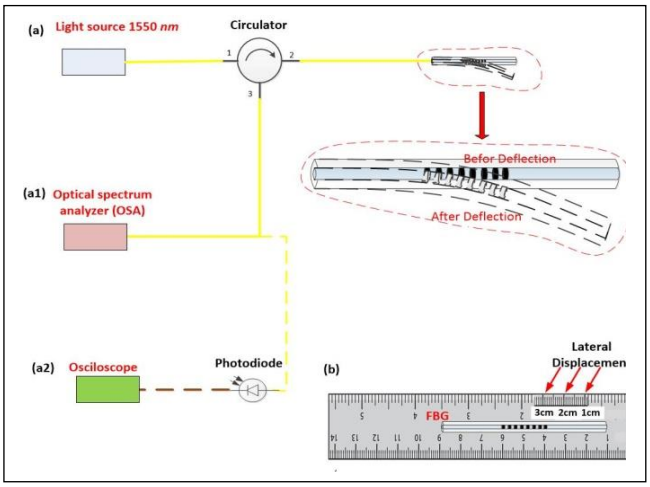

Figure 7 (a) Experiment set up of tension and curvature effect on FBG. (a1) using (OSA) to retrieve the reflected spectrum data. (a2) using oscilloscope to record the change in the voltage, the discrete lines represents using oscilloscope to record the change in the voltage. (b) Location of applied stress

3.0 RESULTS AND DISCUSSION

3.1 Center Wavelength, λ_β shift for various tension and curvature of 10 *mm* FBG.

Figure 8 shows the variation of center wavelength, λ_β with respect to the lateral displacement for the three stress locations. It was noticed that the center wavelength is increased when the displacement is increased. Worthwhile, The slope changed with the location of the applied stress. The values of the aslope at 1 cm, 2 cm and 3 m were found to be 2.0214x10^{-4} *nm/* μm, 2.4854x10^{-4} *nm/* μm and 2.9415x10^{-4} *nm/* μm, respectively, indicating that the sensitivity of the FBG has increased as the stress location became closer to the FBG. Nevertheless, no hysteresis effect was observed at each stress location. This was because there has been no significant change in the slope when the displacement has increased or decreased.

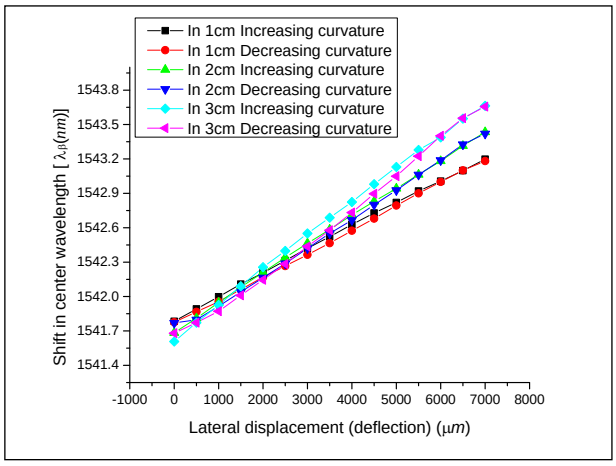

Figure 8 Center wavelength λ_β shift for various tension and curvature of FBG, at different applied stress location, (1cm, 2cm, and 3cm) far away from the end of FBG region

3.2 Output power of reflected signal for various tension and curvature

Figure 9 shows the reflection spectrum received from the OSA for each applied stress location. The result shows a random increase in the width and in the area under the reflected curve, indicating that the power has increased randomly upon the increment of the curvature. As the displacement increases, more power is being reflected.

An increase in the area under reflection curve, estimated by the Origin 9 program, was observed and tabulated in Table 1. By taking into account that the total area represents the total output reflected power coming from the FBG, then it is expected that the output reflected power received by the photodiode is also increased accordingly.

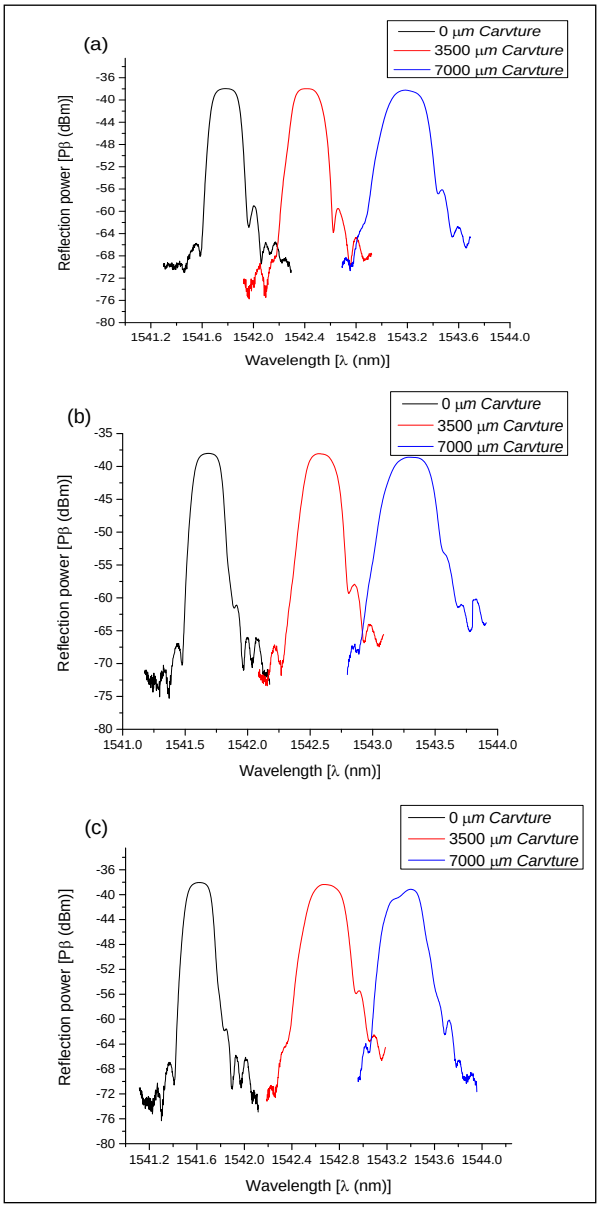

Figure 9 Reflected spectrum power for various tension and curvature of 10 *mm* FBG, at different applied stress location, [a) at 1cm, b) at 2cm, and c) at 3cm] far away from the end of FBG region

Table 1 Increase in area under the reflection curve

Displacement	1cm Location	2cm Location	3cm Location
0 μm	10.62576	12.33524	12.66567
3500 μm	13.37573	15.02563	16.01705
7000 μm	15.15562	20.55292	21.06956

3.3 Reflected Voltage for Various Tension and Curvature of 10 *mm*

Figure 10 shows the plot of average voltage obtained from the oscilloscope against lateral displacement. It is clear from the graph that the output reflected power is increased with increasing lateral displacement. It was evident that the experimental results are in good agreement with the deduced results shown in Table 1, indicating the consistency of both experimental and theoretical measurements.

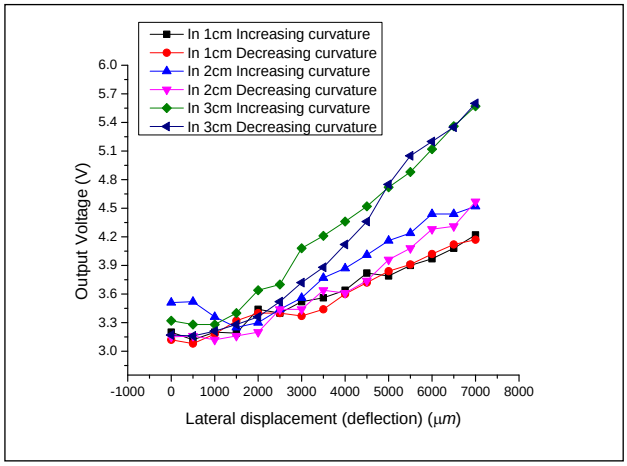

Figure 10 Output voltage for various tension and curvature of 10 *mm* FBG, at different applied stress location, 1cm, 2cm, and 3cm) far away from the end of FBG region

4.0 CONCLUSION

In this work, the response of FBG-bonded plastic plate at different locations of applied stress was investigated. The lateral displacement applied on the plastic ruler bonded with FBG is used to produce increment or decrement in the curvature of the ruler. The main conclusions drawn from the results of this investigation can be summarized as follows:

(a) The sensitivity of the FBG was changed with the location of applied stress. When the stress location approached the location of the FBG, the sensitivity of FBG (in magnitude) increased from 1.542x10^{-4} $V.\mu m^{-1}$, to 3.47x10^{-4} $V.\mu m^{-1}$.

(b) It was seen from the reflection spectrum that the output power was increased randomly when the location of the applied stress approached to the location of the FBG. This was confirmed by the increment in the area of the reflection spectrum. The random increase in the output voltage was attributed to the insufficient stiffness of the plastic ruler, suggesting the implement of graphene plate instead of plastic ruler and increasing the grating length of FBG.

(c) A clear correlation between the optical and electrical outputs has been observed while the increase in the output power was detected by photodiodes.

Acknowledgement

The authors would like to thank the Malaysian Ministry of Higher Education and Universiti Teknologi Malaysia for their financial funding through GUP vote number Q.J130000.2509.08H40. This support is gratefully acknowledged.

References

[1] Hill, K., Fujii, Y., Johnson, D. C. and Kawasaki, B. 1978. Photosensitivity In Optical Fiber Waveguides: Application To Reflection Filter Fabrication. *Applied Physics Letters*. 32(10): 647-649.

[2] Hill, K. O. and Meltz, G. 1997. Fiber Bragg Grating Technology Fundamentals And Overview. *Lightwave Technology, Journal of*. 15(8): 1263-1276.

[3] Skaar, J. 2000. Synthesis And Characterization Of Fiber Bragg Gratings. NTNU. Mastro, S. A. Optomechanical Behavior Of Embedded Fiber Bragg Grating Strain Sensors. Ph.D. Thesis. Drexel University. 2005.

[4] Othonos, A. 1997. Fiber Bragg Gratings. *Review Of Scientific Instruments*. 68(12): 4309-4341.

[5] Matin, M., Hussain, N. and Shoureshi, R. 2005. Fiber Bragg Sensor For Smart Bed Sheet. *Optics & Photonics 2005. International Society for Optics and Photonics*. 590706-590706.

[6] Lin, Y.-B., Lin, T.-K., Kuo, Y.-H., Wang, L. and Chang, K.-C. 2002. Application of FBG Sensors To Strain And Temperature Monitoring Of Full Scale Prestressed Concrete Bridges. *Optical Fiber Sensors Conference Technical Digest, 2002. Ofs 2002, 15th. IEEE*. 211-214.

[7] Li, H.-N., Li, D.-S. and Song, G.-B. 2004. Recent Applications Of Fiber Optic Sensors To Health Monitoring In Civil Engineering. *Engineering Structures*. 26(11): 1647-1657.

[8] Miesen, N., Mizutani, Y., Groves, R. M., Sinke, J. and Benedictus, R. 2011. Lamb Wave Detection In Prepreg Composite Materials With Fibre Bragg Grating Sensors. SPIE Smart Structures and Materials+ Nondestructive Evaluation and Health Monitoring. *International Society For Optics And Photonics*. 79812J-79812J.

[9] Chan, T. H., Yu, L., Tam, H.-Y., Ni, Y.-Q., Liu, S., Chung, W. and Cheng, L. 2006. Fiber Bragg Grating Sensors For Structural Health Monitoring Of Tsing Ma Bridge: Background And Experimental Observation. *Engineering Structures*. 28(5): 648-659.

[10] Seo, D.-C., Yoon, D.-J., Kwon, I.-B. and Lee, S.-S. 2009. Sensitivity Enhancement Of Fiber Optic FBG Sensor For Acoustic Emission. *The 16th International Symposium on: Smart Structures and Materials & Nondestructive Evaluation and Health Monitoring. International Society for Optics and Photonics*. 729415-729415.

[11] Lee, J. R., Chong, S. Y., Yun, C. Y. and Sohn, H. 2010. Design of Fiber Bragg Grating Acoustic Sensor for Structural Health Monitoring of Nuclear Power Plant. *Advanced Materials Research*. 123: 859-862.

[12] Takahashi, N., Hirose, A. and Takahashi, S. 1997. Underwater Acoustic Sensor With Fiber Bragg Grating. *Optical Review*. 4(6): 691-694.

[13] Takahashi, N., Tetsumura, K. and Takahashi, S. 1999. Underwater Acoustic Sensor Using Optical Fiber Bragg Grating As Detecting Element. *Japanese Journal Of Applied Physics*. 38: 3233.

[14] Moccia, M., Pisco, M., Cutolo, A., Galdi, V., Bevilacqua, P. and Cusano, A. 2011. Opto-acoustic Behavior Of Coated Fiber Bragg Gratings. *Optics Express*. 19(20): 18842-18860.
[15] Wild, G. and Hinckley, S. 2010. Optical Fibre Bragg Gratings For Acoustic Sensors. *International Congress on Acoustics (ICA)*. 23–27.
[16] http://www.smartfibres.com/interrogationtechniques.
[17] Lee, B. and Jeong, Y. 2002. Interrogation Techniques For Fiber Grating Sensors And The Theory Of Fiber Gratings. *Fiber Optic Sensors*. 295-381.
[18] Webb, D. J., Surowiec, J., Sweeney, M., Jackson, D. A., Gavrilov, L., Hand, J., Zhang, L. and Bennion, I. 1996. Miniature Fiber Optic Ultrasonic Probe. SPIE's 1996 International Symposium on Optical Science, Engineering, and Instrumentation. *International Society for Optics and Photonics*. 76-80.
[19] Lin, B. and Giurgiutiu, V. 2014. Development Of Optical Equipment For Ultrasonic Guided Wave Structural Health Monitoring. SPIE Smart Structures and Materials+ Nondestructive Evaluation and Health Monitoring. *International Society for Optics and Photonics*. 90620R-90620R.
[20] Perez, I. M., Cui, H. and Udd, E. 2001. Acoustic Emission Detection Using Fiber Bragg Gratings. SPIE's 8th Annual International Symposium on Smart Structures and Materials. *International Society for Optics and Photonics*. 209-215.
[21] Ambrosino, C., Diodati, G., Laudati, A., Gianvito, A., Sorrentino, R., Breglio, G., Cutolo, A., Cusano, A. *et al*. 2007. Active Vibration Control Using Fiber Bragg Grating Sensors And Piezoelectric Actuators In Co-Located Configuration. Third European Workshop on Optical Fibre Sensors. *International Society for Optics and Photonics*. 661940-661940.
[22] Fujisue, T., Nakamura, K. and Ueha, S. 2006. Demodulation Of Acoustic Signals In Fiber Bragg Grating Ultrasonic Sensors Using Arrayed Waveguide Gratings. Japanese *Journal Of Applied Physics*. 45(5S): 4577.
[23] Lin, B. and Giurgiutiu, V. 2013. Exploration of Ultrasonic Guided Wave Detection with Optical Fiber Sensors and Piezoelectric Transducers. *Proc. 9th International Workshop on Structural Health Monitoring, IWSHM*.
[24] Wild, G. and Richardson, S. 2012. Optimisation of Power Detection Interrogation Methods for Fibre Bragg Grating Sensors.